Improving Simulations of Daily Mean Sea Level Extremes in the Gulf of Mexico with High-Resolution Community Earth System Model

Gaopeng Xu[1], Ping Chang[1,2], Gokhan Danabasoglu[3], Frederic S. Castruccio[3], Stephen Yeager[3], Qiuying Zhang[1], Jaison Kurian[1], Susan Bates[4], Christine C. Shepard[5], Justin Small[3]

[1]Department of Oceanography, Texas A&M University, College Station, Texas, USA

[2]Department of Atmospheric Sciences, Texas A&M University, College Station, Texas, USA

[3]NSF National Center for Atmospheric Research, Boulder, Colorado, USA

[4]The Nature Conservancy, Nassawadox, Virginia, USA

[5]The Nature Conservancy, Gulf of Mexico Program, Key West, Florida, USA

Corresponding author: Gaopeng Xu (gaopxu@tamu.edu)

Abstract

Extreme sea-level events, such as those caused by tropical cyclones (TCs), pose significant risks to coastal areas. However, the current generation of climate models struggles to simulate these events due to coarse resolution. By comparing high-resolution (HR) and low-resolution (LR) Community Earth System Model (CESM) simulations with tide gauge and altimeter data along the U.S. Gulf of Mexico (GoM) coast, we find that HR better represents both mean dynamic sea level (DSL) and daily mean extreme DSL (EDSL) statistics. In contrast, LR significantly underestimates the strength of EDSL mainly due to its deficiency in simulating strong TCs. Both observations and HR show larger daily mean EDSL on the western Gulf coast than the eastern side, highlighting the need for HR climate simulations to improve coastal resilience planning.

Keywords: extreme sea levels, tropical cyclones, high-resolution climate models

1. Introduction

Coastal extreme sea level (ESL) is primarily driven by a combination of storm surge and high tide, with contributions from mean sea level and wave runup. It has caused tens of billions of dollars in economic losses due to flood-induced infrastructure [1,2] and ecosystem [3,4] damage in coastal regions. For example, Hurricane Katrina in 2005 produced storm surges ranging from 2.4 m to 8.5 m along the coasts of Alabama, Louisiana, and Mississippi, and these surges penetrated 9 to 20 kilometers inland in many areas. Katrina caused 1,833 fatalities and resulted in $186.3 billion in damages (adjusted for inflation to 2022 dollars) [5,6]. Without any protection strategies, the global-sea-level-rise-induced flooding is projected to cause worldwide annual economic losses ranging from US$21 trillion to US$210 trillion by 2100 [7,8]. As such, evaluating ESL is listed as one of the major objectives of the Intergovernmental Panel on Climate Change (IPCC) Sixth Assessment Report [9]. Therefore, realistically simulating ESL is

crucial to make informed decisions and improve adaptation strategies for the coastal communities.

The Gulf of Mexico (GoM) is one of the hot spots for sea level rise [9–12]. The U.S. coast of GoM has experienced a remarkable 26.1% population growth over the past two decades, the fastest among the U.S. coastal regions. Along the northern GoM coast, weather and sub-seasonal variations have a more significant impact on ESL than tides, seasonal cycles, and interannual-to-decadal variability [13]. Weather-induced ESL is particularly pronounced because GoM is a hurricane intensification region due to its warm waters, especially within warm mesoscale ocean eddies [14–17]. Strong winds associated with hurricanes are the main driver of storm surge in GoM. Additionally, strong coast-parallel winds during hurricanes can drive large sea-level rise through shoreward Ekman transport [18].

However, simulating hurricanes or tropical cyclones (TCs) remains a challenge for standard climate models with a 1º atmosphere resolution. Increasing atmosphere resolution to 0.25º improves simulations of TCs, including their frequency, intensity, and spatial distribution [19]. Coastal ocean geometry and continental shelf features also play an important role in determining the strength of extreme sea-level events [20]. Climate models used in IPCC reports typically feature a 1º ocean resolution and simplified coastline geometry, which limit their ability to simulate sea-level extremes. Increasing the ocean resolution to 0.1º significantly enhances the representation of ocean bathymetry (Figure S1) and western boundary currents, such as the Gulf Stream [21–24]. These improvements can be particularly important for accurately simulating sea levels in GoM.

Here, we assess the impact of horizontal model resolutions on ESL simulations in GoM by comparing an unprecedented ensemble of high-resolution Community Earth System Model (CESM) simulations (Chang et al., 2020, 2023, 2025) with its low-resolution counterpart. The analysis focuses on daily mean extreme dynamic sea-level (EDSL) events, which exclude the effects of high tides and wave runup. These EDSL statistics are valuable for coastal flooding planning, especially in a warming climate, as they provide a baseline understanding of the broader processes driving extreme sea-level changes, even without accounting for tides and wave runup [18].

2. Data and methods

2.1. CESM simulations

Model simulations used in this study were performed with CESM version 1.3 [22,25–27], which consists of the Community Atmosphere Model version 5 (CAM5), the Parallel Ocean Program version 2 (POP2), the Community Land Model version 4 (CLM4), and the Community Ice Code version 4 (CICE4). In the high-resolution CESM (HR), the ocean and sea ice components have a horizontal resolution of 0.1º while the atmosphere and land have a horizontal resolution of 0.25º. In contrast, the low-resolution CESM (LR) has a nominal resolution of 1º for all components.

We use an ensemble of 10 historical and future-transient (HF-TNST) climate simulations covering the period from 1920 to 2100, forced by observed radiative forcing from 1920 to 2005 followed by RCP8.5 forcing from 2006 to 2100 (Chang et al., 2025). The data from 1993 to

2020, corresponding to the satellite data, will be used to compare with observations. Because the ocean model conserves volume, the daily mean DSL has a zero global mean. We note that CESM, even with its HR configuration, does not simulate tides and wave runup. Therefore, the ESL in this study is examined with daily mean DSL anomalies that exclude high tides and wave runup. In the following, the anomalies are referenced to the annual mean of DSL.

2.2. Observations

Two observational datasets are used to validate the CESM simulations. The first is the daily sea surface height above geoid derived from gridded satellite altimetry measurements during the period 1993-2020, known as the Archiving, Validation and Interpretation of Satellite Oceanographic (AVISO) dataset [28]. The second consists of hourly tide gauge (TG) sea level measurements from 13 TG stations along the U.S. GoM coasts (Figure S2) during the same period of 1993-2020, obtained from Global Extreme Sea Level Analysis Version 3 dataset [29–31]. TG data processing steps include 1) removing tides based on Utide Matlab functions [32]; 2) removing contributions from vertical land motion, and barystatic Gravitation, Rotation, and deformation fingerprints estimated by Dangendorf et al. (2023); 3) averaging hourly data into daily means; 4) removing inverse barometer effect based on daily mean sea level pressure from JAR55 [34,35]; 5) conversion to DSL by removing global averaged sea level estimated by Dangendorf et al. (2024). The last two steps above are also applied to the AVISO data for converting to DSL.

2.3. Extreme value theory

EDSL is defined as the yearly maximum of daily mean DSL after removing the annual mean. Without significant sea level rise, EDSL can be treated as a random variable. We use the Generalized Extreme Value (GEV) distribution to estimate 50-year return sea levels, as extreme values converge to GEV under extreme value theory [37,38]. The cumulative probability function (CDF) of the GEV distribution for a random variable x is given by

$$G(x) = exp\left\{-\left[1+\xi\left(\frac{x-\mu}{\sigma}\right)\right]^{-1/\xi}\right\},$$

where μ, σ, and ξ are the location, scale, and shape parameters, respectively. The return period for a given EDSL (x_p) can be estimated by $1/p$, where $p = 1 - G(x \le x_p)$ is the exceedance probability. Similarly, the return level can be obtained for a given return period. This study focuses on the 50-year return sea level, estimating DSLs expected to be equaled or exceeded once every 50 years. Figure S3 displays the well-matched empirical and GEV-fit CDF of EDSL from 13 TG locations, validating the GEV distribution for GoM. To fairly compare with TG, EDSL over 1993-2020 from each ensemble member in HR and LR is fitted to GEV distribution separately.

3. Results

3.1. Comparison of observed and simulated daily mean extreme sea level

To evaluate CESM's capability in simulating large EDSL, we select the ensemble member with the largest daily mean DSL anomalies from 1993 to 2020 (among 10 ensemble members) for

both HR and LR, comparing it with TG and AVISO at each TG station. This ensures consistent DSL data lengths for statistical analysis. The probability density functions (PDFs) of DSL show substantial discrepancies between the TG and AVISO datasets (Figure 1a), with altimetry showing a shorter right tail due to insufficient coastal resolution [39]. This discrepancy can be quantified by comparing the 99th percentile values, which are 28.01 cm in the TG dataset and 20.58 cm in the AVISO dataset. Similarly, LR with 1º horizontal resolution fails to capture the long tail seen in the TG data. In contrast, HR better aligns with TG, with a 99th percentile value of 26.71 cm, suggesting the improved capability of HR to capture realistic EDSL compared to LR. Results remain similar when concatenating all 10 ensemble members to generate histograms (Figure S4a).

We further demonstrate the improvements in HR by analyzing the 50-year return daily mean DSL (DSL50). DSL50 from TG varies spatially from Port Isabel to Key West (Figure 1b), and the 13-station mean is 70.06 cm. However, this is substantially underestimated in AVISO (28.78 cm) and LR (37.51 cm) by 59% and 47%, respectively. In contrast, the mean DSL50 in HR is 72.17 cm, more aligned with TG. The spatial correlation between DSL50 in TG and HR for 13 stations is 0.75 although the TG DSL50 at Cedar Key and St. Petersburg is underestimated by 60% in HR. For LR, the correlation with TG is only 0.63, showing DSL50 larger than 60 cm only at Freeport. Therefore, DSL50 in HR is more realistic than in LR in terms of both amplitudes and spatial variations.

To quantify inter-ensemble variability, we calculate DSL50 spreads in HR and LR (Figure S4b). HR exhibits greater spread along the Texas coast than Florida. For example, at Galveston, the ensemble-mean DSL50 is 82.39 cm, with upper and lower bounds as 114.37 cm and 56.69 cm, respectively. In contrast, at Naples, the corresponding values are 38.14 cm, 47.45 cm, and 31.22 cm, respectively. Except at Cedar Key and St. Petersburg, the TG DSL50 values fall within the HR ensemble spread. However, at most stations, the TG values are above the HR ensemble mean, indicating that HR underestimates observed DSL50. This discrepancy may be partly due to the model biases in TC frequency and intensity [25]. The LR ensemble spreads are considerably smaller than those in HR and are substantially lower than both the TG and HR DSL50 values at all stations. Additionally, DSL50 calculated from 1920-2005 in HR and LR aligns with results from 1993-2020 but exhibits smaller amplitudes (Figure S4c). The analysis including annual means over 1920–2005 shows only minor impacts on DSL50 (Figure S4d). Therefore, we will focus on the 1920–2005 period to further investigate the physical processes driving EDSL in HR and LR without annual means.

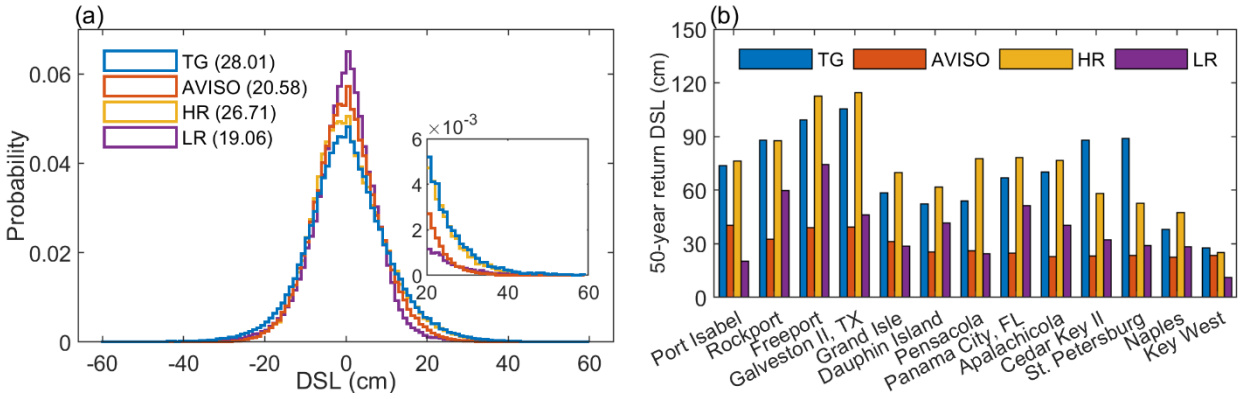

Figure 1 (a) Probability density function of DSL from 13 tide gauge stations along the U.S. GoM coasts (west to east). Numbers in brackets are the 99th percentile of DSL. (b) 50-year return level ESL at tide gauge stations. AVISO, HR, and LR data from 1993 to 2020 are used. Years with fewer than five days of missing data from 1920 to 2020 are used for TG to ensure a comparable sample size with other datasets. Only the ensemble member with the highest DSL from 1993 to 2020 at each TG station is used for HR and LR. Annual mean is removed for all datasets.

3.2. Relationship between Daily mean EDSL and TCs

Because storms are the primary driver of strong EDSL events [20,40], we use self-organizing maps (SOM) [41,42], an unsupervised machine learning technique, to identify storm patterns linked to EDSL events in HR and LR historical ensembles. Specifically, SOM is applied to EDSL and the corresponding daily mean sea level pressure (SLP) data within a 10º×10º box centered on each TG station. A SOM size of 6×1, the dimensions of the neural grid determining how many clusters will be used to represent the input data, is used, and results remain consistent with larger SOM sizes. In contrast, smaller SOM sizes, such as 3×1 or 4×1, fail to sufficiently distinguish strong tropical storms from weaker ones (not shown here).

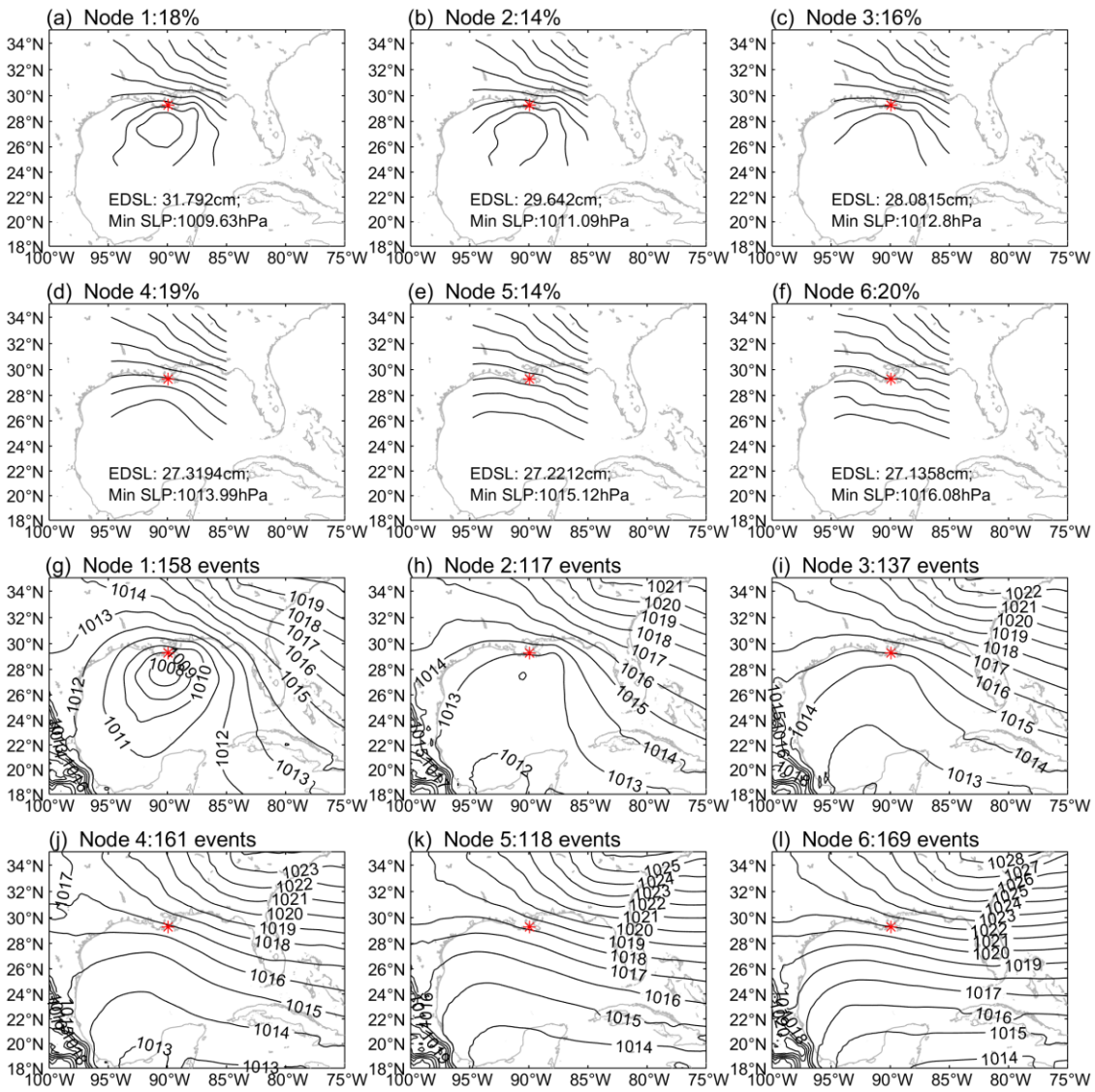

Figure 2 (a-f) Daily mean EDSL at TG station Grand Isle (asterisk) and SLP patterns (dimensionless) in each SOM node. (g-l) Composite SLP for each SOM node (unit: hPa). The percentage (number) of EDSL events identified by different nodes is labelled in a-f (g-l). 10 ensemble members of HR simulations are used.

As an example, the SOM nodes at Grand Isle are shown in Figure 2, revealing both TC and non-TC SLP patterns (Figure 2a-f). Grand Isle is part of the Louisiana coasts, which is vulnerable to TCs. For each SLP snapshot associated with EDSL, the best matching unit ("winner" among the six SOM nodes) is identified based on the minimum Euclidean distance to the snapshot. This process categorizes EDSL events into six groups corresponding to the six SOM nodes. To characterize the SLP patterns in each group, composite SLP maps are presented in Figure 2g-l. Notably, only 18% of EDSL events (158 cases) are linked to TC patterns, as represented by Node 1, while 14% (117 cases) correspond to weaker low-pressure systems captured by Node 2. At most stations, the composite SLP pattern for Node 1 exhibits a clear TC structure, similar to that

at Grand Isle, except at Key West, where a frontal structure dominates (Figure S5). Winter fronts, which occur in December and January, also contribute to EDSL at Grand Isle, especially in Node 6 (Figure S6). At some stations, winter storms have a more pronounced impact on EDSL than at Grand Isle, with a higher frequency of events observed in January and February (Figure S7). Similar SOM results are seen in LR, although the TC-like SLP pattern represented by Node 1 is considerably weaker and broader, indictive of much weaker winds (Figure S8).

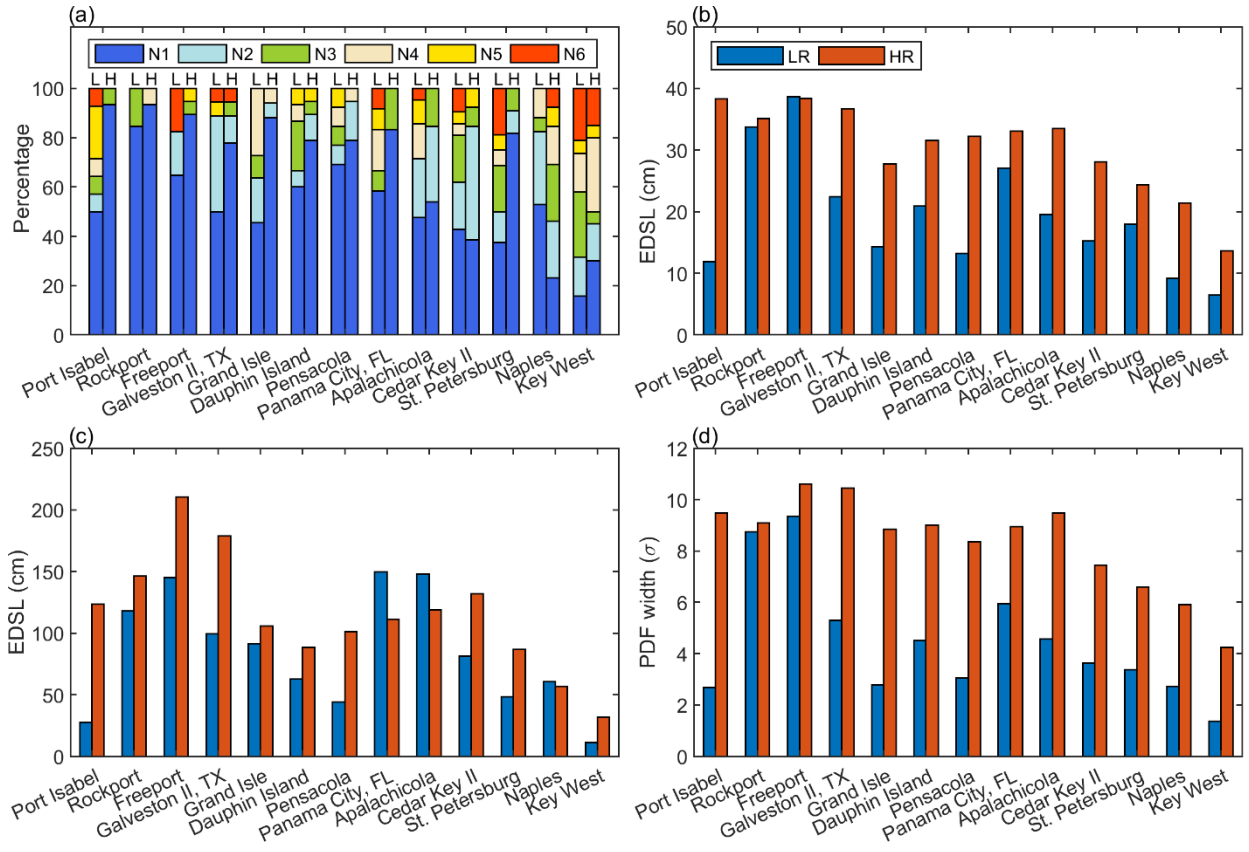

Figure 3 (a) Percentage of severe daily mean EDSL event (larger than DSL50) explained by six SOM nodes in HR (H) and LR (L). (b) Most frequent (i.e. GEV parameter 'location') and (c) strongest daily mean EDSL associated with Node 1 in HR (red) and LR (blue). (d) GEV parameter 'scale' (PDF width) for EDSL events associated with Node 1 in HR (red) and LR (blue). 10 ensemble members of HR and LR simulations are used.

Next, we investigate how severe daily mean EDSL events, defined as those exceeding DSL50, relate to Node 1. As illustrated in Figure 3a, most events align with TC events identified by Node 1 in both LR and HR. In LR, TC contributions reach a maximum of ~85% at Rockport and a minimum of ~15% at Key West, with values at other stations ranging between 40% and 65%. In contrast, HR reveals more intricate spatial patterns, with Node 1 contributions reaching or exceeding 80% along the Texas coast as well as at Grand Isle (Louisiana), Dauphin Island (Alabama), Pensacola (Florida), Panama City (Florida), and St. Petersburg (Florida). Conversely, contributions at Naples and Key West (Florida) fall below 50%, indicating a reduced influence of TCs on EDSL at these stations compared to others.

Histograms and GEV-fit probability density function (PDF) of daily mean EDSL associated with Node 1 are presented in Figure S9, with key parameter information summarized in Figure 3b-d. The GEV parameter 'location' represents the magnitude of the most frequent events. In HR, this parameter is higher along the Texas coast (Port Isabel, Rockport, Freeport, and Galveston), ranging between 35 cm and 40 cm, compared to other regions. In contrast, along the Florida coast from Apalachicola to Key West, it decreases progressively from 33 cm to 14 cm (Figure 3b). Overall, the 13-station mean (standard deviation) of the most frequent EDSL is 30 cm (7 cm).

In HR, daily mean EDSL events exceeding 100 cm occur more frequently west of Grand Isle than east of it. The highest recorded daily mean EDSL event has an amplitude of 211 cm at Freeport, followed by 179 cm at Galveston and 146 cm at Rockport, all situated along the Texas coast (Figure 3c). The strongest daily mean EDSL events at all stations are associated with TCs, with the lowest SLP ranging from 959 hPa to 986 hPa (Figure S10), corresponding to category 1 to 3 hurricanes. Notably, a single hurricane can influence EDSL events at multiple stations simultaneously. For example, the strongest EDSL event at both Freeport and Galveston is driven by the same hurricane. In contrast, the strongest EDSL event at Key West, which has the smallest amplitude, is driven by a hurricane in the North Atlantic rather than GoM. Additionally, the strong spatial correlation (0.96) between GEV parameters 'location' and 'scale' (the width of GEV distribution) suggests that stations experiencing more frequent large EDSL also exhibit a wider range of EDSL (Figure 3d).

In LR, the 13-station mean (standard deviation) of the most frequent daily mean EDSL is only 19 cm (9 cm), making it 37% weaker and 29% more variable than in HR. However, at Rockport and Freeport, the most frequent daily mean EDSL events are comparable to those in HR, warranting further investigation into the underlying cause. Compared to HR, the strongest EDSL event in LR is weaker at most TG stations, except at Panama City and Apalachicola (Figure 3c). A TC with the lowest SLP of 970 hPa drives the strongest EDSL event from Dauphin Island to St. Petersburg, producing an amplitude of 150 cm at Panama City and 148 cm at Apalachicola (Figure S11). Similar to HR, the spatial patterns of the GEV width parameter 'scale' align with those of parameter 'location' in LR, but with a smaller magnitude of parameter 'scale', suggesting a narrower range of EDSL values in LR.

In addition to weather events, low-frequency variability, including intraseasonal and seasonal fluctuations, can also contribute to daily mean EDSL events. To quantify the relative contributions of weather and low-frequency variability, we separated EDSL into a weather-driven component and a low-frequency component. The weather component was extracted by first applying a 15-day high-pass filter to the daily mean DSL time series, then identifying EDSL events in the filtered data using the same timestamps as the original total EDSL events.

The total EDSL associated with Node 1 shows a significant linear relationship with the weather-driven EDSL (Figure S12). From Port Isabel to Pensacola, the slopes of the linear regressions of total EDSL on weather-driven EDSL are close to 1, with correlation coefficients exceeding 0.8 in HR, indicating that high-frequency weather events predominantly drive EDSL. Further east, from Panama City to St. Petersburg, the slopes range between 0.75 and 0.89, with correlation

coefficients between 0.7 and 0.8. At Naples and Key West, the correlations weakened to 0.59 and 0.43, respectively. Overall, the impact of TCs on total EDSL increases from the east to the west across GoM. Compared to HR, LR shows weaker correlations and lower slopes, indicating a reduced influence of weather on EDSL. For example, at Dauphin Island, the correlation in LR is only 0.61, substantially lower than 0.83 in HR. Additionally, total EDSL associated with other nodes generally exhibits lower slopes and weaker correlations with weather-driven EDSL across most tide gauge stations (not shown here).

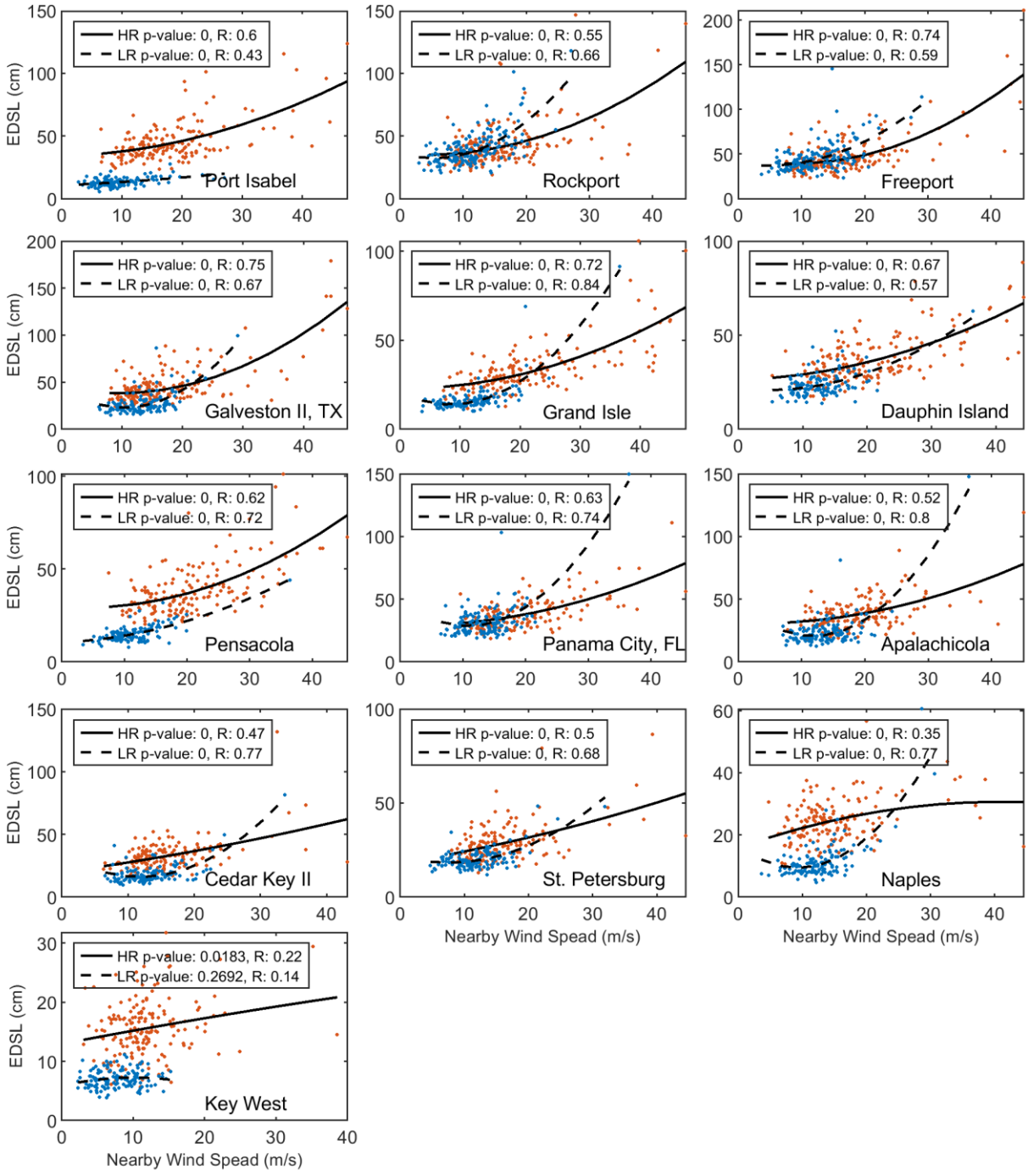

Figure 4 Scatterplots of nearby wind speed (maximum within 2.5º of TG stations) versus total EDSL for Node 1 at 13 TG stations in HR (orange) and LR (blue). Solid and dashed curves show quadratic regression for HR and LR, respectively. Each panel includes P-value and fit correlation. The quadratic fit is statistically significant at 95% confidence, except at Key West. 10 ensemble members of HR and LR simulations are used.

As TCs approach the coast, the sea level change is proportional to U^2W/h in the first order, where U is wind speed, W is the shelf width, and h is the mean depth over the shelf region [20,43]. The surge is mainly generated in shallow regions and is expected to increase with the square of wind speed. Needham & Keim (2014) demonstrated a nonlinear relationship between observed storm surge heights and tropical cyclone wind speeds along the U.S. Gulf Coast. A subsequent numerical modeling study by Yin et al. (2020) revealed that this nonlinear relationship varies by location. Leveraging the 10 ensemble members of CESM simulations, we further investigate this nonlinear relationship in both HR and LR experiments. As shown in Figure 4, daily mean EDSL in HR is significantly correlated with the nearby wind speed (defined as the maximum wind speed within 2.5º to the TG stations) in a quadratic relationship. The fit correlation coefficients reach a maximum of 0.75 at Galveston, followed by Freeport and Grand Isle with values greater than 0.7. On the Florida coast from Cedar Key to Naples, the fit correlation is smaller than 0.5. Additionally, the quadratic relationship at Key West is not significant at 95% confidence level. Notably, this quadratic relationship is sensitive to the geometry of continental shelf, the size [20] and approach direction [46,47] of TCs, as well as the method to construct the wind index [44,46]. In contrast to HR, LR struggles to generate strong winds with amplitudes larger than 20 m/s at most stations (Figure 4). In the weak wind regime, results from LR are nearly indistinguishable from those in HR. However, in the strong wind regime, HR and LR exhibit distinct nonlinear relationships between EDSL and wind speed. Additionally, this relationship is sensitive to the rare severe EDSL events in LR at most stations (Figure S13). This divergence suggests that we cannot simply extrapolate the relationship derived from the weak wind regime to the strong wind regime. Therefore, it is crucial for climate models to permit or resolve strong TCs to better simulate large coastal EDSL in GoM.

4. Conclusions

Our study examines how climate model resolution affects daily mean EDSL simulations along the GoM coast by comparing HR and LR CESM ensembles with TG and altimetry data. TG observations show a higher daily mean DSL50 along the Texas and Louisiana coasts than west Florida, averaging 70.06 cm across 13 stations. HR better captures these spatial variations, underestimating DSL50 by 19%, whereas LR underestimates it by 54% with 10 ensemble member average. Using SOM, we classify daily mean EDSL into six groups, with the most intense events (Node 1) linked to TCs. Catastrophic EDSL events exceeding DSL50 are driven by strong TCs at all TG stations. Since LR simulates weaker TCs than HR, it significantly underestimates EDSL. Additionally, the EDSL PDF is narrower in LR, reflecting poor TC representation.

This study focuses only on the daily mean EDSL because of the limitation of climate model outputs, which may underestimate the short-lived extreme events and wave impacts. In future

work, applying a regional model downscaling approach would be beneficial for investigating hourly EDSL variations associated with storm surges, wave runup, and tides. Nevertheless, our findings highlight the importance of incorporating high-resolution models into policy-making processes to better prepare for and mitigate the impacts of future sea-level rise and extreme weather events. Extending the analysis to future projections will further clarify the influence of tropical cyclone changes on EDSL variability and trends.

Acknowledgments

This research was supported by the National Academies of Science and Engineering (NASEM) Gulf Research Program grant 2000013283 and the NSF grant AGS-2231237. The NSF National Center for Atmospheric Research (NCAR) is a major facility sponsored by the NSF under Cooperative Agreement 1852977. We acknowledge the Texas Advanced Computing Center at The University of Texas at Austin for providing HPC resources on Frontera. We also acknowledge high-performance computing support from Derecho: HPE Cray EX System (https://doi.org/10.5065/qx9a-pg09) provided by NSF NCAR's Computational and Information Systems Laboratory, sponsored by the NSF.

Reference

[1] Hallegatte S, Green C, Nicholls R J and Corfee-Morlot J 2013 Future flood losses in major coastal cities *Nat. Clim. Change* **3** 802–6

[2] Kron W 2013 Coasts: the high-risk areas of the world *Nat. Hazards* **66** 1363–82

[3] Lovelock C E, Feller I C, Reef R, Hickey S and Ball M C 2017 Mangrove dieback during fluctuating sea levels *Sci. Rep.* **7** 1680

[4] Ury E A, Yang X, Wright J P and Bernhardt E S 2021 Rapid deforestation of a coastal landscape driven by sea-level rise and extreme events *Ecol. Appl.* **31** e02339

[5] Knabb R D, Rhome J R and Brown D P 2005 *Tropical cyclone report: Hurricane katrina, 23-30 august 2005* (National Hurricane Center)

[6] Murphy J D 2018 *August/September 2017 Hurricane Harvey*

[7] Hinkel J, Lincke D, Vafeidis A T, Perrette M, Nicholls R J, Tol R S, Marzeion B, Fettweis X, Ionescu C and Levermann A 2014 Coastal flood damage and adaptation costs under 21st century sea-level rise *Proc. Natl. Acad. Sci.* **111** 3292–7

[8] Jevrejeva S, Jackson L, Grinsted A, Lincke D and Marzeion B 2018 Flood damage costs under the sea level rise with warming of 1.5 C and 2 C *Environ. Res. Lett.* **13** 074014

[9] Fox-Kemper B, Hewitt H T, Xiao C, Aðalgeirsdóttir G, Drijfhout S S, Edwards T L, Golledge N R, Hemer M, Kopp R E and Krinner G 2021 Ocean, cryosphere, and sea level change *Climate Change 2021: The Physical Science Basis. Contribution of Working Group*

I to the Sixth Assessment Report of the Intergovernmental Panel on Climate Change (Cambridge University Press) pp 1211–361

[10] Wang J, Church J A, Zhang X, Gregory J M, Zanna L and Chen X 2021 Evaluation of the local sea-level budget at tide gauges since 1958 *Geophys. Res. Lett.* **48** e2021GL094502

[11] Marcos M and Woodworth P L 2017 Spatiotemporal changes in extreme sea levels along the coasts of the N orth A tlantic and the G ulf of M exico *J. Geophys. Res. Oceans* **122** 7031–48

[12] Hu A and Bates S C 2018 Internal climate variability and projected future regional steric and dynamic sea level rise *Nat. Commun.* **9** 1068

[13] Li S, Wahl T, Barroso A, Coats S, Dangendorf S, Piecuch C, Sun Q, Thompson P and Liu L 2022 Contributions of different sea-level processes to high-tide flooding along the US Coastline *J. Geophys. Res. Oceans* **127** e2021JC018276

[14] Goni G, DeMaria M, Knaff J, Sampson C, Ginis I, Bringas F, Mavume A, Lauer C, Lin I-I and Ali M 2009 Applications of satellite-derived ocean measurements to tropical cyclone intensity forecasting *Oceanography* **22** 190–7

[15] Potter H, DiMarco S F and Knap A H 2019 Tropical cyclone heat potential and the rapid intensification of Hurricane Harvey in the Texas Bight *J. Geophys. Res. Oceans* **124** 2440–51

[16] Trenberth K E, Cheng L, Jacobs P, Zhang Y and Fasullo J 2018 Hurricane Harvey links to ocean heat content and climate change adaptation *Earths Future* **6** 730–44

[17] Le Hénaff M, Domingues R, Halliwell G, Zhang J A, Kim H, Aristizabal M, Miles T, Glenn S and Goni G 2021 The role of the Gulf of Mexico ocean conditions in the intensification of Hurricane Michael (2018) *J. Geophys. Res. Oceans* **126** e2020JC016969

[18] Shen J and Gong W 2009 Influence of model domain size, wind directions and Ekman transport on storm surge development inside the Chesapeake Bay: A case study of extratropical cyclone Ernesto, 2006 *J. Mar. Syst.* **75** 198–215

[19] Roberts M J, Camp J, Seddon J, Vidale P L, Hodges K, Vanniere B, Mecking J, Haarsma R, Bellucci A and Scoccimarro E 2020 Impact of model resolution on tropical cyclone simulation using the HighResMIP–PRIMAVERA multimodel ensemble *J. Clim.* **33** 2557–83

[20] Resio D T and Westerink J J 2008 Modeling the physics of storm surges *Phys. Today* **61** 33–8

[21] Sein D V, Koldunov N V, Danilov S, Sidorenko D, Wekerle C, Cabos W, Rackow T, Scholz P, Semmler T and Wang Q 2018 The relative influence of atmospheric and oceanic model resolution on the circulation of the North Atlantic Ocean in a coupled climate model *J. Adv. Model. Earth Syst.* **10** 2026–41

[22] Small R J, Bacmeister J, Bailey D, Baker A, Bishop S, Bryan F, Caron J, Dennis J, Gent P and Hsu H 2014 A new synoptic scale resolving global climate simulation using the Community Earth System Model *J. Adv. Model. Earth Syst.* **6** 1065–94

[23] Xu G, Chang P, Ramachandran S, Danabasoglu G, Yeager S, Small J, Zhang Q, Jing Z and Wu L 2022 Impacts of model horizontal resolution on mean sea surface temperature biases in the community earth system model *J. Geophys. Res. Oceans* **127** e2022JC019065

[24] Li D, Chang P, Yeager S G, Danabasoglu G, Castruccio F S, Small J, Wang H, Zhang Q and Gopal A 2022 The impact of horizontal resolution on projected sea-level rise along US east continental shelf with the Community Earth System Model *J. Adv. Model. Earth Syst.* **14** e2021MS002868

[25] Chang P, Zhang S, Danabasoglu G, Yeager S G, Fu H, Wang H, Castruccio F S, Chen Y, Edwards J and Fu D 2020 An unprecedented set of high-resolution earth system simulations for understanding multiscale interactions in climate variability and change *J. Adv. Model. Earth Syst.* **12** e2020MS002298

[26] Chang P, Xu G, Kurian J, Small R J, Danabasoglu G, Yeager S, Castruccio F, Zhang Q, Rosenbloom N and Chapman P 2023 Uncertain future of sustainable fisheries environment in eastern boundary upwelling zones under climate change *Commun. Earth Environ.* **4** 19

[27] Meehl G A, Yang D, Arblaster J M, Bates S C, Rosenbloom N, Neale R, Bacmeister J, Lauritzen P H, Bryan F and Small J 2019 Effects of model resolution, physics, and coupling on Southern Hemisphere storm tracks in CESM1. 3 *Geophys. Res. Lett.* **46** 12408–16

[28] Hauser D, Tourain C, Hermozo L, Alraddawi D, Aouf L, Chapron B, Dalphinet A, Delaye L, Dalila M and Dormy E 2020 New observations from the SWIM radar on-board CFOSAT: Instrument validation and ocean wave measurement assessment *IEEE Trans. Geosci. Remote Sens.* **59** 5–26

[29] Woodworth P L, Hunter J R, Marcos M, Caldwell P, Menéndez M and Haigh I 2016 Towards a global higher-frequency sea level dataset *Geosci. Data J.* **3** 50–9

[30] Haigh I D, Marcos M, Talke S A, Woodworth P L, Hunter J R, Hague B S, Arns A, Bradshaw E and Thompson P 2023 GESLA version 3: A major update to the global higher-frequency sea-level dataset *Geosci. Data J.* **10** 293–314

[31] Caldwell P, Merrifield M and Thompson P 2015 Sea level measured by tide gauges from global oceans–the Joint Archive for Sea Level holdings (NCEI Accession 0019568), Version 5.5, NOAA National Centers for Environmental Information, Dataset *Cent. Env. Inf. Dataset* **10** V5V40S7W

[32] Codiga D 2020 UTide unified tidal analysis and prediction functions *MATLAB Cent. File Exch.*

[33] Dangendorf S, Hendricks N, Sun Q, Klinck J, Ezer T, Frederikse T, Calafat F M, Wahl T and Törnqvist T E 2023 Acceleration of US Southeast and Gulf coast sea-level rise amplified by internal climate variability *Nat. Commun.* **14** 1935

[34] Kobayashi S, Ota Y, Harada Y, Ebita A, Moriya M, Onoda H, Onogi K, Kamahori H, Kobayashi C and Endo H 2015 The JRA-55 reanalysis: General specifications and basic characteristics *J. Meteorol. Soc. Jpn. Ser II* **93** 5–48

[35] Tsujino H, Urakawa S, Nakano H, Small R J, Kim W M, Yeager S G, Danabasoglu G, Suzuki T, Bamber J L and Bentsen M 2018 JRA-55 based surface dataset for driving ocean–sea-ice models (JRA55-do) *Ocean Model.* **130** 79–139

[36] Dangendorf S, Sun Q, Wahl T, Thompson P, Mitrovica J X and Hamlington B 2024 Probabilistic reconstruction of sea-level changes and their causes since 1900 *Earth Syst. Sci. Data Discuss.* **2024** 1–37

[37] Coles S, Bawa J, Trenner L and Dorazio P 2001 *An introduction to statistical modeling of extreme values* vol 208 (Springer)

[38] DelSole T and Tippett M 2022 *Statistical methods for climate scientists* (Cambridge University Press)

[39] Ballarotta M, Ubelmann C, Pujol M-I, Taburet G, Fournier F, Legeais J-F, Faugère Y, Delepoulle A, Chelton D and Dibarboure G 2019 On the resolutions of ocean altimetry maps *Ocean Sci.* **15** 1091–109

[40] Needham H F, Keim B D and Sathiaraj D 2015 A review of tropical cyclone-generated storm surges: Global data sources, observations, and impacts *Rev. Geophys.* **53** 545–91

[41] Kohonen T 1982 Self-organized formation of topologically correct feature maps *Biol. Cybern.* **43** 59–69

[42] Kohonen T 1990 The self-organizing map *Proc. IEEE* **78** 1464–80

[43] Pugh D and Woodworth P 2014 *Sea-level science: understanding tides, surges, tsunamis and mean sea-level changes* (Cambridge university press)

[44] Needham H F and Keim B D 2014 Correlating storm surge heights with tropical cyclone winds at and before landfall *Earth Interact.* **18** 1–26

[45] Yin J, Griffies S M, Winton M, Zhao M and Zanna L 2020 Response of storm-related extreme sea level along the US Atlantic coast to combined weather and climate forcing *J. Clim.* **33** 3745–69

[46] Lin N, Emanuel K A, Smith J A and Vanmarcke E 2010 Risk assessment of hurricane storm surge for New York City *J. Geophys. Res. Atmospheres* **115**

[47] Weisberg R H and Zheng L 2006 Hurricane storm surge simulations for Tampa Bay *Estuaries Coasts* **29** 899–913